

# Polycatenar pyrazole and pyrazolate ligands as building blocks of new columnar Pd(II) metallomesogens†

Cite this: *Dalton Trans.*, 2014, **43**, 8849

Cristián Cuerva,<sup>a</sup> José A. Campo,<sup>a</sup> Paloma Ovejero,<sup>a</sup> María R. Torres<sup>b</sup> and Mercedes Cano<sup>\*a</sup>

Dicatenar pyridine-functionalised pyrazole ligands [Hpz<sup>R(n,n)py</sup>] (R(n,n) = C<sub>6</sub>H<sub>3</sub>(OC<sub>n</sub>H<sub>2n+1</sub>)<sub>2</sub>, n = 4, 6, 8, 10, 12, 14, 16, 18) have been strategically synthesised to be used as new building blocks for designing discotic liquid crystalline materials. Their coordination to Pd(II) fragments has allowed to achieve two novel families of metallomesogens, [Pd(pz<sup>R(n,n)py</sup>)<sub>2</sub>] (I) and [PdCl<sub>2</sub>(Hpz<sup>R(n,n)py</sup>)] (II), in which the ligand is coordinated in the anionic form as pyrazolate or in the neutral form as pyrazole, respectively. Thermal studies showed that the ligands with n = 14 and 16 carbon atoms, as well as all the palladium complexes, display discotic mesophases in the temperature range of 68–141 °C. The results indicate that the coordination environment around the metal is a determining factor which allows control of the supramolecular arrangement of the mesophase. Disc-like molecules from complexes I pack themselves into cylindrical structures that result in hexagonal columnar phases (Col<sub>h</sub>), while the half-disc shaped molecules from II self-assemble into a layer with an antiparallel dimeric disposition which generates lamellar columnar phases (Col<sub>l</sub>). Schematic models based on X-ray powder diffraction (XRD) experiments are proposed to illustrate the molecular organisation of these Pd metallomesogens in the columnar mesophases.

Received 4th February 2014,  
Accepted 11th April 2014

DOI: 10.1039/c4dt00369a

www.rsc.org/dalton

## Introduction

In recent years, metallomesogens have been one of the major areas of research<sup>1</sup> and a lot of compounds exhibiting mesomorphic properties have been reported and their physical properties studied.<sup>2</sup> In particular, discotic liquid crystals are of great interest due to their high charge-carrier mobility and their one-dimensional aromatic  $\pi$ - $\pi$  stacking,<sup>3,4</sup> which can contribute to their potential applications such as field-effect transistors,<sup>5</sup> photovoltaic solar cells,<sup>6</sup> optical data storage devices,<sup>7</sup> sensors<sup>8–10</sup> and electroluminescent displays.<sup>11</sup>

The formation of supramolecular structures favouring mesomorphic properties depends mainly on the combination of the coordination geometry of metal ions and the nature of ligands.<sup>12,13</sup> Tetracoordinated d<sup>8</sup>-transition metals with a

square-planar geometry are likely to achieve disc-like molecules that allow to attain favourable columnar stacking arrangements for inducing mesomorphism. So, molecular systems containing Pd(II),<sup>14,15</sup> Pt(II)<sup>16,17</sup> or Ni(II)<sup>18</sup> have been found to exhibit columnar liquid crystal properties. However, in 1986, for the first time a new series of disc-like copper complexes was reported which exhibited both columnar and layered stacking in the mesophase.<sup>19</sup> Since then, few metallomesogens have been prepared and characterised with lamellar columnar mesophases (Col<sub>l</sub>).<sup>20–23</sup>

On the other hand, pyrazole ligands have been proved to be good candidates to induce mesomorphism in their coordination to different metal centres. Pyrazole is an electron-rich ligand with weak  $\pi$ -accepting and strong  $\sigma$ -donating properties as pyrazole derivatives are easily deprotonated to form anionic species.<sup>24</sup> A strategy used in the design of metallomesogens is to incorporate functionalised bridging pyrazolates due to their ability to attain an adequate geometry for achieving mesomorphic properties. In this context, pyrazole and pyrazolate palladium,<sup>25,26</sup> gold<sup>27–29</sup> and silver<sup>10,30</sup> complexes have been described as liquid crystal materials with smectic and columnar arrangements.

Recently, we have reported Ag(I)<sup>10</sup> and Zn(II)<sup>31</sup> metallomesogens based on monocatenar pyridine-functionalised pyrazoles which have been demonstrated to be excellent building blocks to induce smectic behaviour. The presence of the pyridine moiety

<sup>a</sup>Departamento de Química Inorgánica I, Facultad de Ciencias Químicas, Universidad Complutense, E-28040 Madrid, Spain. E-mail: mmcano@ucm.es; Fax: +34 91394 4352; Tel: +34 91394 4340

<sup>b</sup>Laboratorio de Difracción de Rayos-X, Facultad de Ciencias Químicas, Universidad Complutense, E-28040 Madrid, Spain

†Electronic supplementary information (ESI) available: Full characterisation of the pyrazole ligands and their corresponding Pd(II) metallomesogens, selected bond distances and angles for **1** and **12**, PLUTO molecular drawing for **17** and X-ray crystallographic data in CIF format for **1** and **12**. CCDC 977934 and 977935. For ESI and crystallographic data in CIF or other electronic format see DOI: 10.1039/c4dt00369a

**Table 1** Numbering of the compounds described in this work

Compound <sup>a</sup>	Type	<i>n</i>	Number		
[Hpz <sup>R(n,n)py</sup> ]		4	1		
		6	2		
		8	3		
		10	4		
		12	5		
		14	6		
		16	7		
		18	8		
[Pd(pz <sup>R(n,n)py</sup> ) <sub>2</sub> ]	<b>I</b>	4	9		
		6	10		
		8	11		
		10	12		
		12	13		
		14	14		
		16	15		
		18	16		
		[PdCl <sub>2</sub> (Hpz <sup>R(n,n)py</sup> )]	<b>II</b>	4	17
				6	18
8	19				
10	20				
12	21				
14	22				
16	23				
18	24				

<sup>a</sup> R(*n,n*) = C<sub>6</sub>H<sub>3</sub>(OC<sub>n</sub>H<sub>2n+1</sub>)<sub>2</sub>.

in the rigid core enables modification of the molecular geometry and polarisation, thus influencing the mesomorphic behaviour.

In the present work, we describe the synthesis and characterisation of a novel series of dicatenar pyridine-functionalised pyrazole ligands, 3-(3,5-bis(alkyloxy)phenyl)-(5-pyridin-2-yl)pyrazole [Hpz<sup>R(n,n)py</sup>] (R(*n,n*) = C<sub>6</sub>H<sub>3</sub>(OC<sub>n</sub>H<sub>2n+1</sub>)<sub>2</sub>, *n* = 4, 6, 8, 10, 12, 14, 16, 18), and their corresponding palladium metallomesogens [Pd(pz<sup>R(n,n)py</sup>)<sub>2</sub>] and [PdCl<sub>2</sub>(Hpz<sup>R(n,n)py</sup>)]. The square-planar environment around the metal centre as well as the use of the above-mentioned ligands are useful for obtaining disc-like molecules, which are properly organised to form columnar mesophases. The introduction of two alkyloxy chains in each pyrazole ligand has contributed to the formation of these self-assemblies. On the other hand, the results show that the ordering of the disc-like molecules in the mesophases significantly depends on the coordination environment around the metal. So, the palladium complexes prepared with a 2 : 1 (ligand : metal) molar ratio show hexagonal columnar phases (Col<sub>h</sub>), while those with a 1 : 1 relation exhibit lamellar columnar mesophases (Col<sub>L</sub>). In addition, the length of the terminal chains constitutes a very important factor to achieve stable mesophases in a wide range of temperatures.

All the new compounds described in this work (1–24) are schematically presented in Table 1, including the numbering used to identify them.

## Results and discussion

### Synthesis and characterisation

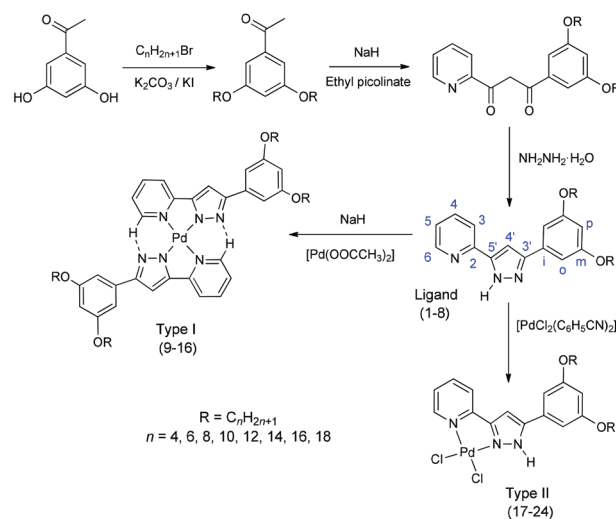
Dicatenar pyridylpyrazole ligands [Hpz<sup>R(n,n)py</sup>] 1–8 were synthesised by a procedure similar to that described for related

monocatenar ones.<sup>10</sup> Reactions of 1–8 with palladium(II) acetate or bis(benzonitrile)dichloridepalladium(II) in a 2 : 1 or 1 : 1 (ligand : metal) molar ratio yielded the new square-planar complexes [Pd(pz<sup>R(n,n)py</sup>)<sub>2</sub>] 9–16 (type **I**) and [PdCl<sub>2</sub>(Hpz<sup>R(n,n)py</sup>)] 17–24 (type **II**), respectively (Scheme 1). All compounds 1–24 were characterised by spectroscopic techniques (IR, <sup>1</sup>H-NMR and <sup>13</sup>C-NMR in some representative cases) and CHN elemental analyses. Some ligands and complexes were obtained with molecules of ethanol or dichloromethane of solvation, respectively (see the Experimental section and ESI†).

The IR spectra of palladium complexes 9–24 in the solid state show the characteristic absorption bands from the ligands, which are slightly shifted in relation to free pyrazoles. Among them, the overlapped ν(C=N) and ν(C=C) bands of the pyridine and pyrazole heterocycles around 1595 cm<sup>-1</sup> and the γ(CH) band corresponding to the deformation of the pyridine group at *ca.* 766 cm<sup>-1</sup> were remarkable. In addition, bands to *ca.* 3190 cm<sup>-1</sup> from the NH-pyrazole group were also observed for 17–24, confirming the neutral nature of the ligand in these compounds. By contrast, their absence in 9–16 agrees with their coordinative form as a pyrazolate group.

The <sup>1</sup>H-NMR spectra of all ligands and compounds in CDCl<sub>3</sub> solution at room temperature, as well as the <sup>13</sup>C-NMR spectra of the ligands 1–8 and derivatives 10, 13 and 18, 21 as representative examples of complexes **I** and **II**, display the expected resonances.

Particularly, in the <sup>1</sup>H-NMR spectra of the complexes **I** the 6-H signal (*ca.* 10.40 ppm) is down-field shifted with respect to that observed in the free pyrazoles (*ca.* 8.64 ppm). This shift is attributed not only to the coordination of the pyridine group to the Pd(II) metal centre, but also to the formation of intramolecular hydrogen bonds (C–H...N) as was observed in the crystal structure of [Pd(pz<sup>R(10,10)py</sup>)<sub>2</sub>] 12, which is described later. Moreover, the presence of unique signals for each type of protons or carbons in the <sup>1</sup>H and <sup>13</sup>C spectra indicates the equivalence of the two pyridylpyrazole ligands.



**Scheme 1** Synthesis of the ligands and complexes. The atom numbering is used in the NMR assignments.

In addition, for compounds **II** the characteristic NH signal of the pyrazole ligands is observed in the  $^1\text{H-NMR}$  at *ca.* 11.20 ppm according to the neutral nature of the coordinated ligand.

It is also interesting to note that the chemical shift of the 4'-H proton of the pyrazole ring is slightly modified in compounds **II**, but is up-field shifted for **I**, which is also associated with the anionic aromatic nature of the ligand in these compounds.

### Crystal structure of $[\text{Hpz}^{\text{R}(4,4)\text{py}}] \mathbf{1}$

Single crystals suitable for X-ray diffraction experiments were obtained by vapour diffusion of hexane into a solution of the ligand in dichloromethane. The molecular structure of **1** is depicted in Fig. 1 and selected bond distances and angles are given in Table S1 in the ESI.† The compound crystallises in the monoclinic system, space group  $P2_1/n$ , with four formula units per unit cell.

The bond distances in the pyrazole, pyridine and benzene rings evidence a delocalised  $\pi$  system. The benzene group is practically coplanar with the pyrazole ring (dihedral angle of  $5.1(1)^\circ$ ), while the pyridine group is slightly rotated with respect to the pyrazole ring (dihedral angle of  $11.2(1)^\circ$ ). The N1 and N3-donor atoms are *cis*-located, unlike the *trans* positions that they occupy in related 1-pyridylpyrazoles.<sup>32</sup> The alkyl chains located at the 3- and 5-positions of the benzene ring show the characteristic C–C distances corresponding to single bonds. The two terminal chains are practically situated on the plane of the own benzene ring (torsion angles of *ca.*  $180^\circ$ ).

One remarkable characteristic is the presence of intermolecular N–H $\cdots$ N hydrogen bonds between the NH group at the pyrazole ring and the N-pyrazolic atom of the neighbouring molecule (N1 $\cdots$ N2, 2.899(3) Å;  $\angle(\text{N1-H1}\cdots\text{N2})$ ,  $142.8^\circ$ ; symmetry operation:  $-x + 2, -y, -z + 1$ ), giving rise to the formation of dimers (see the inset in Fig. 1). The two molecules of the dimer adopt a head-to-tail conformation which is responsible for the disc-like molecular shape of this compound, in contrast with the elongated shape of monocatenar pyrazoles  $[\text{Hpz}^{\text{R}(n)\text{py}}]$  described previously by us.<sup>10</sup>

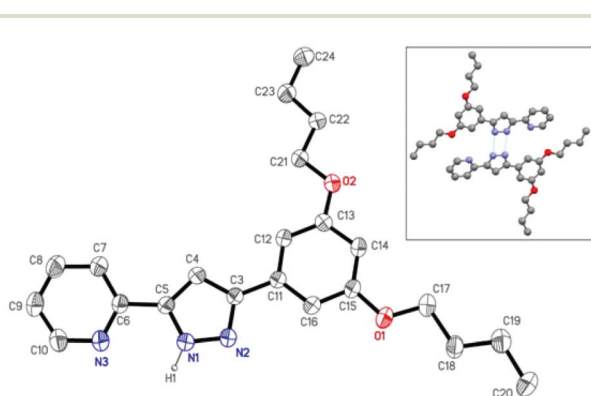


**Fig. 1** ORTEP plot for  $[\text{Hpz}^{\text{R}(4,4)\text{py}}] \mathbf{1}$  with 20% probability. Hydrogen atoms, except H1, have been omitted for clarity. The inset shows the dimeric units defined by hydrogen bonds.

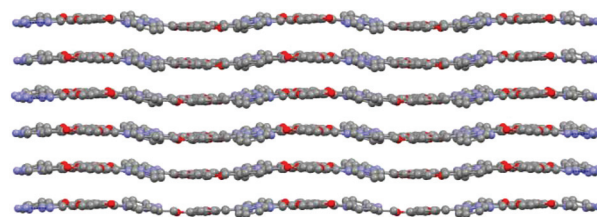


**Fig. 2** Packing of  $[\text{Hpz}^{\text{R}(4,4)\text{py}}] \mathbf{1}$  through the *a*-axis.

The dimeric units are arranged in a layered structure, exhibiting an extensive interdigitation of the alkyl chains (Fig. 2).

### Crystal structure of $[\text{Pd}(\text{pz}^{\text{R}(10,10)\text{py}})_2] \mathbf{12}$

Suitable crystals of **12** were obtained by slow vapour diffusion of acetone into a chloroform solution of the complex. The compound crystallises in the triclinic system, space group  $P\bar{1}$ , with the Pd atom located in the centre of inversion. The molecular structure is depicted in Fig. 3, and Table S2 (see the ESI†) lists selected bond distances and angles.

The palladium atom adopts a tetracoordination defined by four nitrogen atoms of the two pyrazolate ligands, giving rise to an almost square-planar environment. The Pd–N1 and Pd–N3 distances of 1.929(7) and 2.041(7) Å, respectively, are consistent with those observed in related compounds.<sup>33</sup> The major deviation from the ideal geometry is imposed by the bite N1–Pd–N3 angle of  $78.5(4)^\circ$ . The bidentate coordination of the ligand generates an almost planar five-membered metalocycle PdN1C5C6N3 (maximum deviation of 0.019(1) Å for N1), which is coplanar to the coordination plane PdN1N3N1'N3' defined by the metal centre and the four nitrogen atoms of the two bidentate ligands (dihedral angle of  $1.3(4)^\circ$ ).

Pyridine and benzene rings are also coplanar with the pyrazolate one (dihedral angles of  $0.6(1)$  and  $3.9(1)^\circ$ , respectively). The lower value of these angles with respect to those observed in the corresponding free ligand may be associated with an increased conjugation and delocalisation of the  $\pi$  electronic charge as a result of their coordination to the metal centre in

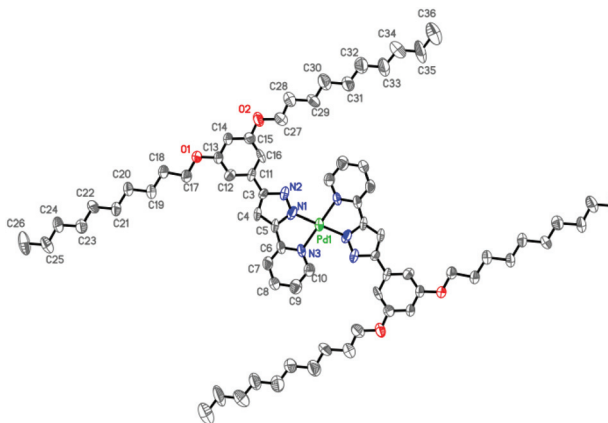


**Fig. 3** ORTEP plot for  $[\text{Pd}(\text{pz}^{\text{R}(10,10)\text{py}})_2] \mathbf{12}$  with 40% probability. Hydrogen atoms have been omitted for clarity.

the pyrazolate form. The C5–C6 and C3–C11 distances of 1.46(2) Å are slightly shorter than in the free pyrazole, in agreement with the above proposal.

The substituent alkyl chains show the characteristic C–C distances associated with single bonds. They are almost coplanar with the benzene ring, as deduced from the angle of *ca.* 85° between the normal to the benzene plane and the line that connects the extremes of each chain.

An important feature was the establishment of intramolecular hydrogen bonds (C–H...N) between the free nitrogen atom at the pyrazolate ring and the nearest carbon atom from the pyridine group of the other ligand (C10...N2, 3.047(1) Å; <(C10–H10...N2), 143.5°; symmetry operation:  $-x + 1, -y + 1, -z + 1$ ) (Fig. 4). These bonds appear to be maintained in solution as is deduced from the chemical shift observed for the 6-H proton in the <sup>1</sup>H-NMR spectra. The pyrazolate ligands adopt a *trans*-arrangement with their terminal alkyl chains pointed in opposite directions and located all parallel to each other. In summary, the molecular structure contains an almost planar rigid core surrounded by four peripheral chains, thus defining a suitable molecular shape to achieve the supramolecular ordering of the observed mesophases.

In addition, each molecular unit is related with their neighbours by weak  $\pi$ ... $\pi$  interactions of *ca.* 3.4 Å involving the pyridine group and benzene rings of neighbouring molecules, thus generating columns along the *a*-axis (Fig. 5). Molecules are displaced from each other, so that the palladium centres are located at 6.79(1) Å. In this situation, the core is rotated 40.3(1)° with respect to the axis defined by the palladium atoms.

Molecular packing can be described as a columnar stacking of molecules, in such a way that the terminal chains of neighbouring columns exhibit extensive interdigitation (Fig. 6). This

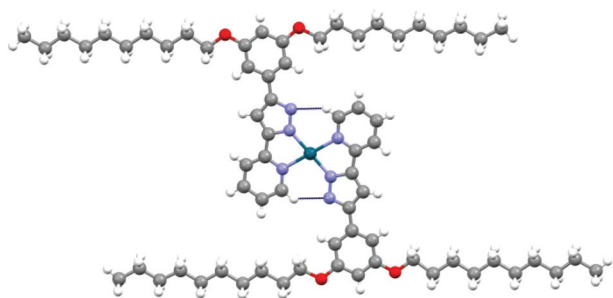


Fig. 4 Disc-like core showing the hydrogen bonds.

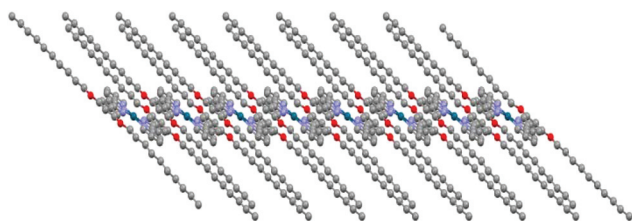


Fig. 5 Column formed by  $\pi$ ... $\pi$  interactions along *a*-axis.

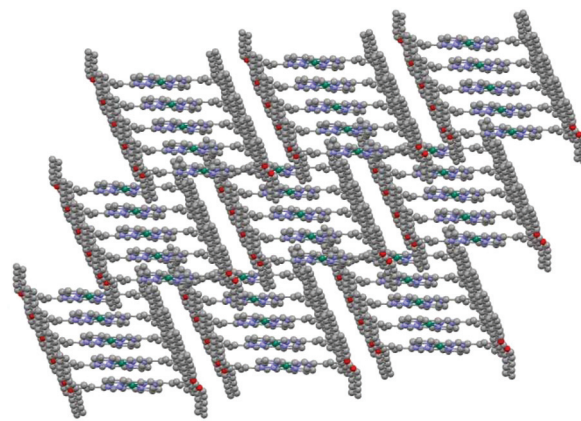


Fig. 6 Packing of [Pd(pz<sup>R(10,10)py</sup>)<sub>2</sub>] **12** through the *a*-axis.

packing may be related to the mesomorphic behaviour observed in these derivatives (see Thermal behaviour) and constitutes a support to propose the existence of a structural relationship between the mesophase and the solid state.

### Thermal behaviour

Thermal properties of the compounds were studied by polarised optical microscopy (POM), differential scanning calorimetry (DSC) and X-ray diffraction at variable temperature (XRD), the latter one used only in representative complexes. Tables 2 and 3 list the phase transition temperatures and their associated enthalpy data established by DSC.

Ligands **6** and **7** displayed enantiotropic liquid crystal properties showing a fibrous texture (Fig. 7), which was similar to that previously reported for the Col<sub>L</sub> mesophase of *meso-tetra* (4-alkylamidophenyl)porphyrin liquid crystals.<sup>34</sup> The remain-

Table 2 Phase behaviour of ligands **1–8** determined by POM and DSC

	<i>n</i>	Transition <sup>a</sup>	<i>T</i> <sup>b</sup> /°C	$\Delta H$ /kJ mol <sup>-1</sup>
<b>1</b>	4	Cr→I	100	29.3
		I→Cr	63 <sup>c</sup>	
<b>2</b>	6	Cr→I	105	46.5
		I→Cr	38 <sup>c</sup>	
<b>3</b>	8	Cr→I	88	36.5
		I→Cr	35 <sup>c</sup>	
<b>4</b>	10	Cr→I	89	54.4
		I→Cr	34 <sup>c</sup>	
<b>5</b>	12	Cr→I	67	50.5
		I→Cr	38 <sup>c</sup>	
<b>6</b>	14	Cr→Col <sub>L</sub>	81 <sup>c</sup>	76.5 <sup>d</sup>
		Col <sub>L</sub> →I	83	
		I→Col <sub>L</sub>	32 <sup>c</sup>	
		Col <sub>L</sub> →Cr	27 <sup>c</sup>	
<b>7</b>	16	Cr→Col <sub>L</sub>	84 <sup>c</sup>	92.6 <sup>d</sup>
		Col <sub>L</sub> →I	86	
		I→Col <sub>L</sub>	35 <sup>c</sup>	
		Col <sub>L</sub> →Cr	30 <sup>c</sup>	
<b>8</b>	18	Cr→I	85	48.2
		I→Cr	40 <sup>c</sup>	

<sup>a</sup>Cr = crystalline phase, Col<sub>L</sub> = lamellar columnar mesophase, I = isotropic liquid. <sup>b</sup>DSC onset peaks. <sup>c</sup>Detected by POM. <sup>d</sup>Overlapped processes.

Table 3 Phase behaviour of Pd(II) complexes determined by POM and DSC

<i>n</i>	[Pd(pz <sup>R(n,n)py</sup> ) <sub>2</sub> ]				[PdCl <sub>2</sub> (Hpz <sup>R(n,n)py</sup> )]			
	Compounds I	Transition <sup>a</sup>	<i>T</i> <sup>b</sup> /°C	Δ <i>H</i> /kJ mol <sup>-1</sup>	Compounds II	Transition <sup>a</sup>	<i>T</i> <sup>b</sup> /°C	Δ <i>H</i> /kJ mol <sup>-1</sup>
4	9	Cr→Cr'→Col <sub>h</sub>	141 <sup>c</sup>	117.4	17	Cr→Col <sub>L</sub>	134	22.0
		Col <sub>h</sub> →I	285	2.8		Col <sub>L</sub> →I	262 <sup>e</sup>	20.8
		I→Col <sub>h</sub>	284	-2.0		I→Col <sub>L</sub>	226	-15.5
		Col <sub>h</sub> →Cr	112	13.6		Col <sub>L</sub> →Cr	111 <sup>d</sup>	
6	10	Cr→Col <sub>h</sub>	99	53.8	18	Cr→Col <sub>L</sub>	120	17.6
		Col <sub>h</sub> →I	269	2.5		Col <sub>L</sub> →I	248	23.0
		I→Col <sub>h</sub>	269	-2.3		I→Col <sub>L</sub>	232	-20.6
		Col <sub>h</sub> →Cr	99	-7.5		Col <sub>L</sub> →Cr	106 <sup>d</sup>	
8	11	Cr→Cr'	64	19.6	19	Cr→Col <sub>L</sub>	103	56.1
		Cr'→Col <sub>h</sub>	90	16.7		Col <sub>L</sub> →I	228	22.9
		Col <sub>h</sub> →I	246	3.5		I→Col <sub>L</sub>	199	-12.1
		I→Col <sub>h</sub>	246	-1.9		Col <sub>L</sub> →Cr	92 <sup>d</sup>	
10	12	Col <sub>h</sub> →Cr	82	-1.4	20	Cr→Cr'	61	2.9
		Cr→Col <sub>h</sub>	80	80.6		Cr'→Col <sub>L</sub>	68	10.9
		Col <sub>h</sub> →I	234	2.2		Col <sub>L</sub> →I	199	13.7
		I→Col <sub>h</sub>	230	-1.3		I→Col <sub>L</sub>	187	-14.7
12	13	Col <sub>h</sub> →Cr	65 <sup>d</sup>		Col <sub>L</sub> →Cr	58 <sup>d</sup>		
		Cr→Cr'→Col <sub>h</sub>	88 <sup>c</sup>	98.6	Cr→Cr'	70	17.2	
		Col <sub>h</sub> →I	204	1.1	Cr'→Col <sub>L</sub>	82	22.0	
		I→Col <sub>h</sub>	204	-0.9	Col <sub>L</sub> →I	190	9.0	
14	14	Col <sub>h</sub> →Cr	60 <sup>d</sup>		I→Col <sub>L</sub>	164	-4.3	
		Cr→Cr'	83	2.5	Col <sub>L</sub> →Cr	74	-21.6	
		Cr'→Col <sub>h</sub>	95	121.4	Cr→Cr'→Col <sub>L</sub>	90 <sup>c</sup>	55.8	
		Col <sub>h</sub> →I	206	2.4	Col <sub>L</sub> →I	188	13.2	
16	15	I→Col <sub>h</sub>	205	-1.9	I→Col <sub>L</sub>	159	-13.6	
		Col <sub>h</sub> →Cr	60 <sup>d</sup>		Col <sub>L</sub> →Cr	78	-29.5	
		Cr→Cr'	76	56.2	23	Cr→Cr'	75	0.7
		Cr'→Col <sub>h</sub>	96	142.4		Cr'→Col <sub>L</sub>	93	13.9
Col <sub>h</sub> →I	187	1.2	Col <sub>L</sub> →I	157 <sup>e</sup>		0.6		
I→Col <sub>h</sub>	186	-1.5	I→Col <sub>L</sub>	135 <sup>d</sup>				
18	16	Col <sub>h</sub> →Cr	73	-59.6	Col <sub>L</sub> →Cr	89 <sup>d</sup>		
		Cr→Cr'	74	30.3	24	Cr→Cr'	78	1.6
		Cr'→Col <sub>h</sub>	102	147.0		Cr'→Col <sub>L</sub>	97	20.1
		Col <sub>h</sub> →I	177	1.3		Col <sub>L</sub> →I	160 <sup>e</sup>	1.0
I→Col <sub>h</sub>	176	-1.3	I→Col <sub>L</sub>	138 <sup>d</sup>				
		Col <sub>h</sub> →Cr	60 <sup>d</sup>		Col <sub>L</sub> →Cr	90 <sup>d</sup>		

<sup>a</sup> Cr, Cr' = crystalline phases, Col<sub>h</sub> = hexagonal columnar mesophase, Col<sub>L</sub> = lamellar columnar mesophase, I = isotropic liquid. <sup>b</sup> DSC onset peaks. <sup>c</sup> Overlapped processes. <sup>d</sup> Detected by POM. <sup>e</sup> Partial decomposition.



Fig. 7 Microphotograph of [Hpz<sup>R(16,16)py</sup>] 7 at 85.4 °C on heating.

ing ligands were not liquid crystals, showing the melting point at temperatures below 105 °C.

In order to establish the nature of this mesophase, a contact preparation study of 6 with the phases of the palla-

dium complexes I and II, which have been unequivocally characterised in this work (see below), was carried out. So, POM observations revealed that the mesophase of 6 was not miscible with the Col<sub>h</sub> phase of 12 but it was with the Col<sub>L</sub> phase of 20, thus confirming the columnar lamellar nature of the mesophase of the pyrazole ligands.

The mesomorphic behaviour of the new ligands [Hpz<sup>R(n,n)py</sup>] contrasts with that observed in the related monocatena pyrazoles of the type [Hpz<sup>R(n)py</sup>], which exhibited smectic mesophases.<sup>10</sup> The increase of the number of terminal chains has been used as a strategy to produce a disc-like molecular shape and to reduce melting points.

In general, the palladium complexes show crystalline polymorphism and enantiotropic liquid crystal behaviour, exhibiting the characteristic optical textures of discotic phases. The melting point was easily detected on heating by the appearance of a phase with intense birefringence and high mobility. For complexes I, the formation of the mesophase from the

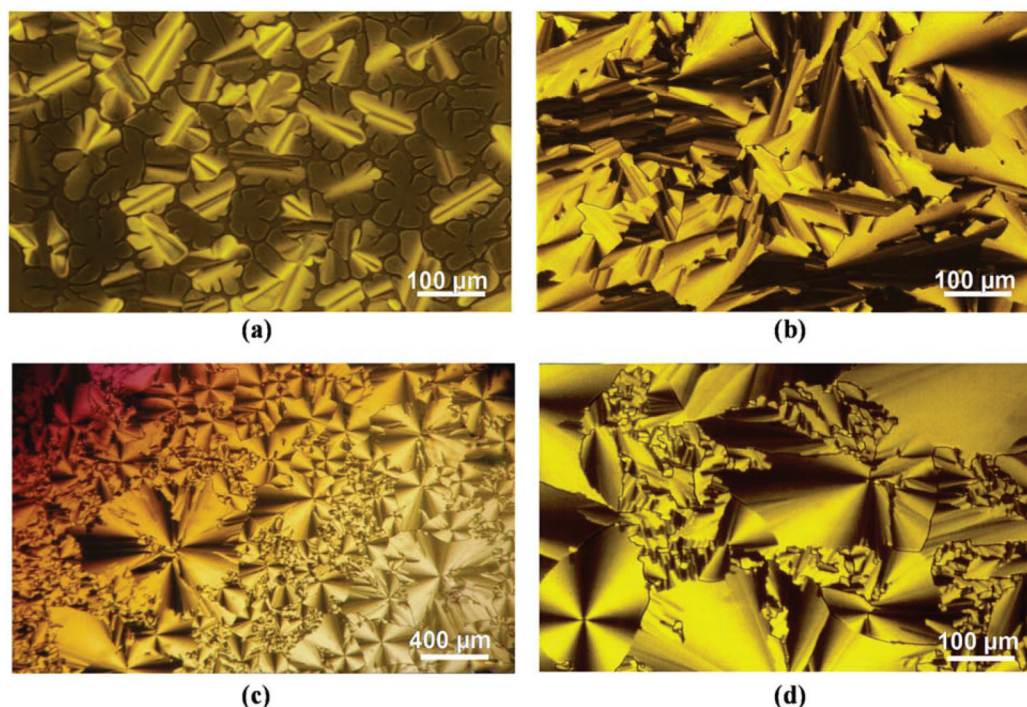


Fig. 8 Microphotographs of (a)  $[\text{Pd}(\text{pz}^{\text{R}(12,12)\text{py}})_2]$  **13** at 192 °C, (b)  $[\text{Pd}(\text{pz}^{\text{R}(12,12)\text{py}})_2]$  **13** at 183 °C, (c)  $[\text{Pd}(\text{pz}^{\text{R}(14,14)\text{py}})_2]$  **14** at 164 °C and (d)  $[\text{Pd}(\text{pz}^{\text{R}(14,14)\text{py}})_2]$  **14** at 127 °C, on cooling (type I).

isotropic liquid gave rise to a dendritic texture with linear birefringent defects, which slowly grew at lower temperatures to form a pseudo-focal conic texture typical of  $\text{Col}_h$  mesophases (Fig. 8).<sup>35</sup> By contrast, a broken fan-like texture was observed for complexes **II**, suggesting lamellar columnar structures (Fig. 9). Similar textures were also found in  $\text{Col}_L$  mesophases of  $\text{Ni}(\text{II})$ <sup>21</sup> and  $\text{Pt}(\text{II})$ <sup>23</sup> complexes previously reported in the literature.

DSC studies support the above results. So, the thermograms of **6** and **7** show a single broad endothermic peak at *ca.* 87 °C in the first heating cycle, which involves overlapped solid-mesophase and mesophase-isotropic liquid transitions in agreement with the POM observations (Fig. S1†). On the other hand, the pronounced hysteresis determined from the tran-

sition temperatures is consistent with the viscous nature observed in the mesophase.

In general terms, the DSC traces of complexes **I** show on heating three endothermic peaks corresponding to solid–solid, solid–mesophase and mesophase–isotrope phase transitions, respectively. In particular, complexes **9** and **13** melt immediately after the solid–solid transformation, so that the two first peaks are overlapped.

Also, the exothermic peak after the solid–solid process was remarkable, which can be perfectly observed in the thermograms of complexes **14** and **16** ( $\Delta H = -11.3$  and  $-32.9$   $\text{kJ mol}^{-1}$ , respectively). This fact suggests that this transformation occurs to give rise to a more stable solid phase through Pd–Pd interactions, achieving a supramolecular organisation suitable for the development of hexagonal columnar mesophases. On cooling, the peak corresponding to the isotrope–mesophase process was detected at temperatures close to the clearing. However, the peak from the mesophase–solid transition was not registered in the thermograms of complexes with long alkyl chains (except for **15**), probably due to the slow solidification process as observed by POM.

The DSC thermograms of complexes **II** with long alkyl chains (**20–24**) show on heating three endothermic peaks corresponding to the solid–solid, solid–mesophase and mesophase–isotrope phase transitions. By contrast, only two peaks consistent with the melting and clearing points were observed in complexes **17–19**. On cooling, the formation of mesophase is established in most cases from the exothermic peak registered at the highest temperatures. Mesophase–solid phase



Fig. 9 Microphotograph of  $[\text{PdCl}_2(\text{Hpz}^{\text{R}(14,14)\text{py}})]$  **22** at 153 °C on cooling (type II).

transition could not be observed probably due to the involvement of a slow transition to a more organised phase. In addition, the hysteresis observed in these complexes suggests the presence of severe restrictions, which makes difficult the molecular mobility and, consequently, the formation of the mesophase on cooling.

In order to discuss the thermal behaviour of both types of compounds, two effects were taken into account, the coordination environment and the alkyl chain length. According to the first one, the melting points of the pyrazolate complexes **I** are only slightly higher than those of the dichloride compounds **II** (except when  $n = 6$  and 8), while the clearing temperatures are significantly higher. This fact suggests a greater packing efficacy in the hexagonal columnar phases of **I**, probably due to greater electronic delocalisation on the molecular core and to stronger intermolecular core–core interactions, which provide greater molecular stability in the  $\text{Col}_h$  phases. As a consequence of these variations on the melting and clearing temperatures, the mesophase stability ranges of **I** are higher than those obtained in the compounds **II** for any chain length (Fig. 10).

On the other hand, the influence of the alkyl chain length on the liquid crystal properties is the same for the two families of compounds **I** and **II**. When the number of the carbon atoms is small, the melting temperatures decrease by increasing the chain length. However, in compounds with  $n > 10$  the van der Waals interactions among the hydrophobic tails are greater by increasing the chain length, thus making the melting temperatures increase. In contrast, the clearing points always decrease

by increasing the length of the alkyl chains, giving rise to the widest mesophase stability ranges when the alkyl chains are the shortest, complexes **10** and **20** exhibiting the highest stability interval.

### Variable-temperature powder X-ray diffraction studies

Selected mesomorphic derivatives of families **I** and **II** were subjected to variable-temperature powder XRD experiments to confirm the hexagonal and lamellar columnar nature of the mesophases observed by POM. Calculated values of Bragg's spacing ( $d_{\text{calc.}}$ ) were obtained from the reciprocal spacing ratio characteristic for hexagonal and lamellar symmetry considering the first peak observed as the (100) and (001) reflection, respectively. Lattice constants were calculated in order to study the supramolecular organisation in the columnar phases.<sup>36</sup> The results are summarised in Table 4.

Diffraction patterns of compound **16**, selected as a representative example of the type **I** complexes were registered in the first heating cycle (Fig. 11). As can be seen, the XRD pattern shows the existence of the phases that were established from POM and DSC studies. So, the diffraction patterns obtained at temperatures at which the liquid crystal state is reached (blue colour in Fig. 11) display a strong fundamental reflection in the low-angle region assigned to (100) with a Bragg's spacing ( $d$ ) of 26.54 Å, followed by a set of weak reflections ( $d = 15.44, 13.38, 10.25$  Å) with a  $d$ -spacing ratio of  $1 : 1/\sqrt{3} : 1/\sqrt{4} : 1/\sqrt{7}$  corresponding to (110), (200) and (210) reflections of a hexagonal columnar phase.

The intracolumnar distance generated by the  $\pi \cdots \pi$  stacking between mesogenic units of each column is evident from the (001) reflection which appears in the high-angle region with a  $d$ -spacing of 3.4 Å. The relationship between the molecular

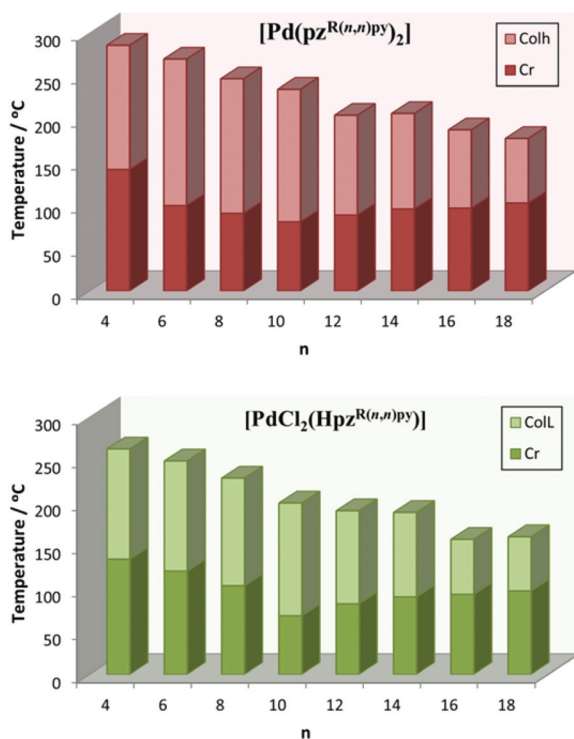


Fig. 10 Bar diagram showing the range of the phases present in the complexes of each family.

Table 4 X-Ray diffraction data

	Phase	$2\theta$ (°)	$d_{\text{meas}}^a$ (Å)	$[hkl]^b$	$d_{\text{calc}}^a$ (Å)	Parameters <sup>c</sup>
<b>16</b>	$\text{Col}_h$	3.3	26.5	100	26.5	$T = 105$ °C
		5.7	15.4	110	15.3	$a = 31$ Å
		6.6	13.4	200	13.3	$V_{\text{mol}} = 2691$ Å <sup>3</sup>
		8.6	10.2	210	10.0	$S_{\text{col}} = 829$ Å <sup>2</sup>
		26.2	3.4	001	—	
		20.0	4.5	—	—	
<b>17</b>	$\text{Col}_L$	5.5	16.1	001	16.1	$T = 160$ °C
		11.0	8.0	002	8.0	$d = 16.1$ Å $V_{\text{mol}} = 929$ Å <sup>3</sup> $A_{\text{mol}} = 115$ Å <sup>2</sup>
<b>22</b>	$\text{Col}_L$	2.9	30.0	001	30.0	$T = 110$ °C
		5.8	15.2	002	15.0	$d = 30.3$ Å
		8.7	10.1	003	10.0	$V_{\text{mol}} = 1367$ Å <sup>3</sup>
		20.0	4.5	—	—	$A_{\text{mol}} = 90$ Å <sup>2</sup>

<sup>a</sup>  $d_{\text{meas}}$  and  $d_{\text{calc}}$  are the measured and calculated diffraction spacings. <sup>b</sup>  $[hkl]$  are the Miller indices of the reflections. <sup>c</sup> Molecular volume:  $V_{\text{mol}} = M_w/(N_A\rho)$ , where  $M_w$  is the molecular weight,  $N_A$  is Avogadro's number and  $\rho$  is the density ( $\sim 1$  g cm<sup>-3</sup>). For hexagonal columnar phases: lattice constant  $a = \sum d_{hk} \sqrt{(h^2 + k^2 + hk)} / \sqrt{(3N_{hk})}$ , where  $N_{hk}$  is the number of  $hk0$  reflections; columnar cross-section area  $S_{\text{col}} = (\sqrt{3}a^2)/2$ . For lamellar columnar phases: lamellar periodicity  $d = (\sum |d_{00l}|)N_{00l}$ , where  $N_{00l}$  is the number of  $00l$  reflections; molecular cross-section area  $A_{\text{mol}} = 2V_{\text{mol}}/d$ .

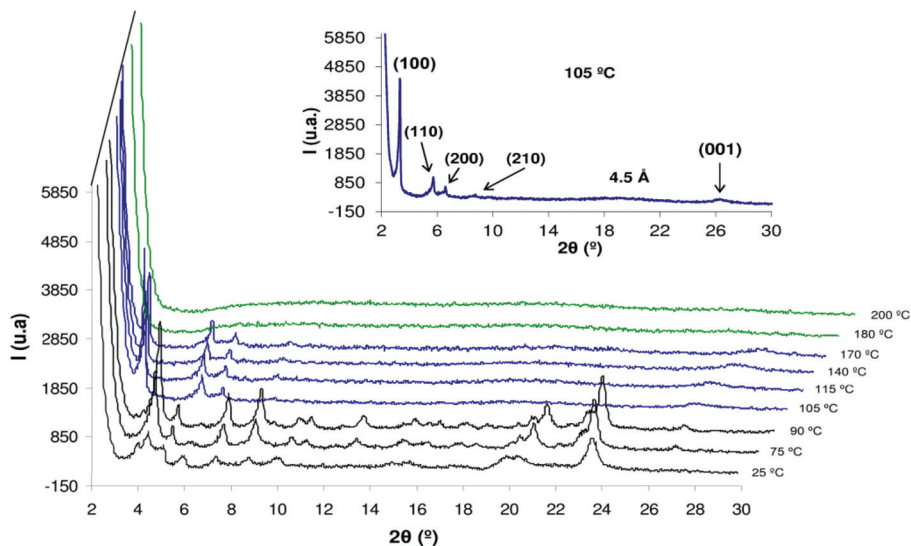


Fig. 11 Powder 2D XRD diffraction pattern for the compound  $[\text{Pd}(\text{pz}^{\text{R}(18,18)\text{py}})_2]$  **16** showing solid (black), liquid crystalline (blue) and liquid (green) phases. A detail of indexed reflections at 105 °C can be observed in the inset.

volume ( $V_m$ ) and the columnar cross-section area ( $S_{\text{col}}$ ) is consistent with the stacking distance observed above; this value suggests the existence of a long-range order along the columns and, consequently, a highly ordered mesophase (Fig. 12a).

In addition, a broad diffuse peak centred at 20.0 Å corresponds to the liquid-like order of the molten terminal chains. It is interesting to note that they can adopt different conformations around the rigid core due to their high mobility in the liquid crystalline phases. The length of the alkyl chains ( $L_n$ ) was estimated from the distances measured in the molecular structure, and is *ca.* 21.1 Å. However, the difference established between the intercolumnar distance ( $a$ ) and the diameter of

the core ( $L_{\text{core}}$ ) was significantly lower, of *ca.* 13 Å. The comparison of both values suggests that the terminal chains present high interdigitation or non-linear conformations in the  $\text{Col}_h$  phases.<sup>37</sup>

On the other hand, the  $\text{Col}_L$  mesophases observed by POM in complexes **II** was confirmed from the diffractogram of **22**, which display at 110 °C the (001), (002) and (003) reflections of a lamellar columnar phase with a  $d$ -spacing ratio of 1 : 1/2 : 1/3, respectively. In addition, a diffuse band was localised in the wide-angle region around 20°, indicating the liquid-like order of the molten chains. However, for complex **17** only two reflections with a Bragg's spacing of 16.10 and 8.01 Å indexed to the (001) and (002) reflections from the  $\text{Col}_L$  mesophase could be observed.

The lamellar periodicity ( $d$ ) measured for the  $\text{Col}_L$  phases in **17** and **22** were 16.1 and 30.3 Å, respectively. Again in both cases, the values of molecular volume ( $V_{\text{mol}}$ ) and cross-section area ( $A_{\text{mol}}$ ) are in perfect agreement with a lamellar structure (see Table 4).

On this basis, we propose that the half-disc shaped molecules of compounds **II** should be arranged into layers but with an antiparallel disposition driven by Pd–Pd interactions, which should account for their columnar packing (Fig. 12b).

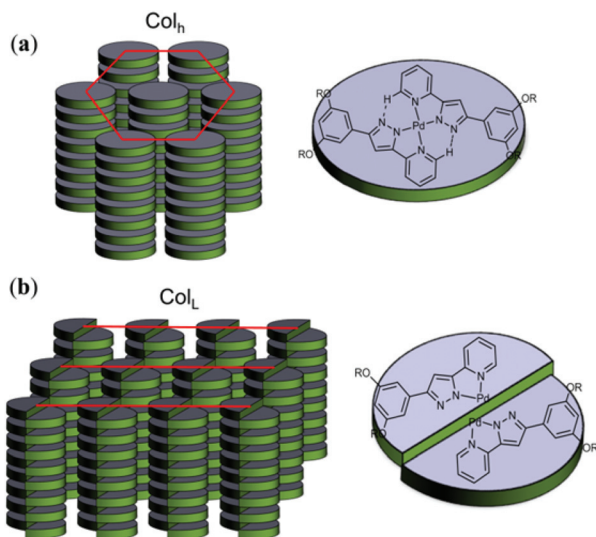


Fig. 12 Proposed schematic model representing the (a) columnar hexagonal and (b) columnar lamellar packing in the mesophase for compounds **I** and **II**, respectively. Chloride atoms have been omitted for clarity.

## Conclusions

A new series of dicatena pyridylpyrazole ligands  $[\text{Hpz}^{\text{R}(n,n)\text{py}}]$  and their corresponding palladium(II) derivatives  $[\text{Pd}(\text{pz}^{\text{R}(n,n)\text{py}})_2]$  and  $[\text{PdCl}_2(\text{Hpz}^{\text{R}(n,n)\text{py}})]$  were prepared and characterised. Thermal studies revealed that those ligands having long alkyl chains at the  $\text{C}_6\text{H}_3(\text{OC}_n\text{H}_{2n+1})_2$  substituents ( $n = 14$  and 16) display enantiotropic discotic mesomorphism to temperatures of *ca.* 80 °C in contrast with the monotropic smectic behaviour observed for the related monocatena pyrazoles  $[\text{Hpz}^{\text{R}(n)\text{py}}]$  in

agreement with their elongated shape. The ionic nature of the ligands in  $[\text{Pd}(\text{pz}^{\text{R}(n,n)\text{py}})_2]$  favours the formation of non-conventional intramolecular hydrogen bonds (C–H...N), stabilizing a head-to-tail disposition of the coordinated ligands and generating a rigid metalocyclic core with a disc-like shape.

The existence of  $\pi\cdots\pi$  lateral interactions of 3.4 Å between the pyridine and benzene rings of neighbouring molecules gives rise to columns that run along the *a* crystallographic axis, as was established from the crystalline structure of **12**. In agreement with the above results, all Pd(II)-bispyrazolate complexes exhibit hexagonal columnar mesophases (Col<sub>h</sub>) in wide temperature ranges. On the other hand, the half-disc shape of  $[\text{PdCl}_2(\text{Hpz}^{\text{R}(n,n)\text{py}})]$  also allows to achieve the supramolecular organisation of the liquid crystal state through the inverted arrangement of molecules in layers, leading to lamellar columnar mesophases (Col<sub>L</sub>).

In summary, the liquid crystal behaviour of the studied compounds significantly depends on both factors, the coordination environment and the alkyl chains length. Results show that the increase of the core–core and van der Waals interactions are determining factors for attaining adequate ordering in the mesophase.

## Experimental section

### Materials and physical measurements

All commercial reagents were used as supplied. The starting Pd(II) compounds were purchased from Sigma-Aldrich. The new 3,5-*n*-dialkyloxyacetophenone compounds were synthesised by alkylation of 3,5-dihydroxyacetophenone with the corresponding derivative  $\text{C}_n\text{H}_{2n+1}\text{Br}$  in acetone solution as previously described for related compounds.<sup>38</sup> These compounds were characterised by analytical and spectroscopic techniques.

Elemental analyses for carbon, hydrogen and nitrogen were carried out by the Microanalytical Service of Complutense University (validated range: %C 0.5–94.7, %H 0.5–7.6, %N 0.5–23.0). IR spectra were recorded on a Perkin Elmer Spectrum 100 FTIR spectrophotometer with a universal ATR accessory in the 4000–650  $\text{cm}^{-1}$  region: w (weak), m (medium) and s (strong). <sup>1</sup>H- and <sup>13</sup>C-NMR spectra were performed at room temperature on a Bruker DPX-300 spectrophotometer (NMR Service of Complutense University) from solutions in  $\text{CDCl}_3$ . Chemical shifts  $\delta$  are listed relative to  $\text{Me}_4\text{Si}$  using the signal of the deuterated solvent as a reference (7.26 and 77.0 ppm for <sup>1</sup>H and <sup>13</sup>C, respectively) and coupling constants *J* are in hertz. Multiplicities are indicated as s (singlet), d (doublet), t (triplet), q (quartet), qt (quintet), ddd (doublet of doublets of doublets), m (multiplet). The <sup>1</sup>H and <sup>13</sup>C chemical shifts are accurate to  $\pm 0.01$  and  $\pm 0.1$  ppm, respectively, and coupling constants to  $\pm 0.3$  Hz.

Phase studies were carried out by optical microscopy using an Olympus BX50 microscope equipped with a Linkam THMS 600 heating stage. The temperatures were assigned on the basis of optic observations with polarised light. Measurements of the transition temperatures were made using a Perkin

Elmer Pyris 1 differential scanning calorimeter with the sample (1–4 mg) sealed hermetically in aluminium pans and with a heating or cooling rate of 10  $\text{K min}^{-1}$ . The X-ray diffractograms at variable temperature were recorded on a Panalytical X'Pert PRO MPD diffractometer with Cu-K $\alpha$  (1.54 Å) radiation in a  $\theta$ – $\theta$  configuration equipped with an Anton Paar HTK1200 heating stage (X-Ray Diffraction Service of Complutense University).

### Synthesis of the compounds

**Ligands 3-(3,5-bis(alkyloxy)phenyl)-(5-pyridin-2-yl)pyrazole [Hpz<sup>R(n,n)py</sup>] (1–8).** To a solution of the corresponding 3,5-*n*-dialkyloxyacetophenone (3.72 mmol) in dry THF (100 mL) was carefully added 60% NaH (7.81 mmol, 0.31 g). The reaction mixture was stirred for 1 h at room temperature. Then, ethyl picolinate (3.72 mmol, 0.56 g) was added and the solution was refluxed for 24 h. The mixture was cooled at room temperature and then 10 mL of methanol were incorporated to quench the excess of NaH. Evaporation of the solvent afforded a residue which was dissolved in ethyl acetate (100 mL), and acidified to pH = 4–5 with dilute HCl 0.2 M. The mixture was washed with water (3  $\times$  50 mL) and dried upon anhydrous magnesium sulphate. After taking the reaction mixture to dryness, a brown residue corresponding to  $\beta$ -diketone was obtained.

Without further purification, to a solution of the corresponding  $\beta$ -diketone (1.12 mmol) in 100 mL of ethanol, hydrazine monohydrate (1.12 mmol, 56 mg) was slowly added. The mixture was stirred for 24 h at 80 °C and then cooled at 4 °C. The white precipitate obtained was filtered off and dried *in vacuo*.

All compounds were characterised by IR, <sup>1</sup>H and <sup>13</sup>C-NMR spectroscopies and elemental analyses (deposited as ESI†). Specific examples of the characterisation are given below.

**[Hpz<sup>R(6,6)py</sup>] (2).** Colourless solid (74%). Found: C, 73.3; H, 8.5; N, 9.6.  $\text{C}_{26}\text{N}_3\text{H}_{35}\text{O}_2 \cdot 0.3\text{EtOH}$  requires C, 73.1; H, 8.1; N, 9.7%.  $\nu_{\text{max}}/\text{cm}^{-1}$  3207w  $\nu(\text{N-H})$ , 1589s  $\nu(\text{C}=\text{C} + \text{C}=\text{N})$ , 789m  $\gamma(\text{C-H})_{\text{py}}$ .  $\delta_{\text{H}}$  (300 MHz;  $\text{CDCl}_3$ ;  $\text{Me}_4\text{Si}$ ): 0.90 (6H, t, <sup>3</sup>*J* 7.0, CH<sub>3</sub>), 1.24 (t, <sup>3</sup>*J* 7.0, EtOH), 1.34 (8H, m, CH<sub>2</sub>), 1.45 (4H, m, CH<sub>2</sub>), 1.79 (4H, qt, <sup>3</sup>*J* 6.7, CH<sub>2</sub>), 3.74 (q, <sup>3</sup>*J* 7.0, EtOH), 4.00 (4H, t, <sup>3</sup>*J* 6.6, OCH<sub>2</sub>), 6.45 (1H, t, <sup>4</sup>*J* 2.2, H<sub>p</sub>), 6.97 (2H, d, <sup>4</sup>*J* 2.2, H<sub>o</sub>), 7.06 (1H, s, 4'-H), 7.26 (1H, m, 5-H), 7.79 (1H, m, 3-H), 7.79 (1H, m, 4-H), 8.63 (1H, d, <sup>3</sup>*J* 4.7, 6-H).  $\delta_{\text{C}}$  (75.48 MHz;  $\text{CDCl}_3$ ;  $\text{Me}_4\text{Si}$ ): 14.0 (CH<sub>3</sub>), 22.5 (CH<sub>2</sub>), 25.6 (CH<sub>2</sub>), 29.2 (CH<sub>2</sub>), 31.5 (CH<sub>2</sub>), 68.0 (OCH<sub>2</sub>), 100.7 (C-4'), 101.4 (C<sub>p</sub>), 104.0 (C<sub>o</sub>), 120.1 (C-3), 122.7 (C-5), 134.1 (C<sub>i</sub>), 136.9 (C-4), 144.9 (C-3'), 148.8 (C-2), 149.3 (C-6), 151.1 (C-5'), 160.5 (C<sub>m</sub>).

**[Hpz<sup>R(12,12)py</sup>] (5).** Colourless solid (74%). Found: C, 77.0; H, 10.1; N, 7.0.  $\text{C}_{38}\text{N}_3\text{H}_{59}\text{O}_2 \cdot 0.2\text{EtOH}$  requires C, 76.8 H, 9.6; N, 7.1%.  $\nu_{\text{max}}/\text{cm}^{-1}$  3159, 3148, 3104w  $\nu(\text{N-H})$ , 1592s  $\nu(\text{C}=\text{C} + \text{C}=\text{N})$ , 778m  $\gamma(\text{C-H})_{\text{py}}$ .  $\delta_{\text{H}}$  (300 MHz;  $\text{CDCl}_3$ ;  $\text{Me}_4\text{Si}$ ): 0.88 (6H, t, <sup>3</sup>*J* 6.9, CH<sub>3</sub>), 1.24 (t, <sup>3</sup>*J* 7.0, EtOH), 1.26 (36H, m, CH<sub>2</sub>), 1.79 (4H, qt, <sup>3</sup>*J* 6.6, CH<sub>2</sub>), 3.72 (q, <sup>3</sup>*J* 7.0, EtOH), 4.00 (4H, t, <sup>3</sup>*J* 6.4, OCH<sub>2</sub>), 6.46 (1H, t, <sup>4</sup>*J* 2.2, H<sub>p</sub>), 6.97 (2H, d, <sup>4</sup>*J* 2.1, H<sub>o</sub>), 7.08 (1H, s, 4'-H), 7.27 (1H, m, 5-H), 7.77 (1H, m, 3-H), 7.77 (1H, m, 4-H), 8.64 (1H, d, <sup>3</sup>*J* 4.8, 6-H).  $\delta_{\text{C}}$  (75.48 MHz;  $\text{CDCl}_3$ ;  $\text{Me}_4\text{Si}$ ): 14.1 (CH<sub>3</sub>), 22.7–31.9 (CH<sub>2</sub>), 68.1 (OCH<sub>2</sub>), 100.6 (C-4'), 101.4

(C<sub>p</sub>), 104.2 (C<sub>o</sub>), 120.0 (C-3), 122.7 (C-5), 134.1 (C<sub>i</sub>), 137.0 (C-4), 144.6 (C-3'), 148.6 (C-2), 149.4 (C-6), 151.6 (C-5'), 160.6 (C<sub>m</sub>).

**Complexes [Pd(pz<sup>R(n,n)py</sup>)<sub>2</sub>] (9–16).** To a solution of the corresponding pyrazole [Hpz<sup>R(n,n)py</sup>] (0.44 mmol) in 40 mL of CH<sub>2</sub>Cl<sub>2</sub> was added 60% NaH (0.88 mmol, 35.2 mg). After 30 min of stirring at room temperature, a solution of [Pd(OOCCH<sub>3</sub>)<sub>2</sub>] (0.22 mmol, 49.37 mg) in 3 mL of CH<sub>2</sub>Cl<sub>2</sub> was added under a nitrogen atmosphere. The reaction was refluxed for 24 h and then cooled at room temperature to yield a precipitate which dissolved in CHCl<sub>3</sub> (20 mL). The solution was filtered over celite and concentrated until a solid begins to precipitate. The yellow compound obtained was filtered off, washed with acetone and dried *in vacuo*.

All compounds were characterised by IR, <sup>1</sup>H spectroscopies and elemental analyses (deposited as ESI†). In addition, complexes **10** and **13** were also characterised by <sup>13</sup>C-NMR as representative examples of this family.

[Pd(pz<sup>R(6,6)py</sup>)<sub>2</sub>] (**10**). Yellow solid (68%). Found: C, 65.9; H, 7.2; N, 8.9. PdC<sub>52</sub>N<sub>6</sub>H<sub>68</sub>O<sub>4</sub> requires C, 65.7; H, 7.0; N, 9.0%.  $\nu_{\max}/\text{cm}^{-1}$  1593s  $\nu(\text{C}=\text{C} + \text{C}=\text{N})$ , 761m  $\gamma(\text{C}-\text{H})_{\text{py}}$ .  $\delta_{\text{H}}$  (300 MHz; CDCl<sub>3</sub>; Me<sub>4</sub>Si): 0.94 (12H, t, <sup>3</sup>J 6.8, CH<sub>3</sub>), 1.39 (16H, m, CH<sub>2</sub>), 1.52 (8H, m, CH<sub>2</sub>), 1.85 (8H, qt, <sup>3</sup>J 6.8, CH<sub>2</sub>), 4.09 (8H, t, <sup>3</sup>J 6.9, OCH<sub>2</sub>), 6.42 (2H, t, <sup>4</sup>J 2.1, H<sub>p</sub>), 6.79 (2H, s, 4'-H), 7.04 (4H, d, <sup>4</sup>J 2.1, H<sub>o</sub>), 7.11 (2H, ddd, <sup>3</sup>J 7.5, 5.4, <sup>4</sup>J 1.3, 5-H), 7.43 (2H, d, <sup>3</sup>J 7.8, 3-H), 7.67 (2H, ddd, <sup>3</sup>J 7.5, 7.8, <sup>4</sup>J 1.3, 4-H), 10.24 (2H, d, <sup>3</sup>J 5.4, 6-H).  $\delta_{\text{C}}$  (75.48 MHz; CDCl<sub>3</sub>; Me<sub>4</sub>Si): 14.1 (CH<sub>3</sub>), 22.7 (CH<sub>2</sub>), 25.8 (CH<sub>2</sub>), 29.4 (CH<sub>2</sub>), 31.7 (CH<sub>2</sub>), 68.0 (OCH<sub>2</sub>), 99.5 (C-4'), 100.0 (C<sub>p</sub>), 103.7 (C<sub>o</sub>), 118.0 (C-3), 120.0 (C-5), 136.9 (C<sub>i</sub>), 138.3 (C-4), 149.4 (C-3'), 149.9 (C-2), 150.6 (C-6), 153.2 (C-5'), 160.2 (C<sub>m</sub>).

[Pd(pz<sup>R(12,12)py</sup>)<sub>2</sub>] (**13**). Yellow solid (78%). Found: C, 71.1; H, 9.1; N, 6.5. PdC<sub>76</sub>N<sub>6</sub>H<sub>116</sub>O<sub>4</sub> requires C, 71.0; H, 8.8; N, 6.6%.  $\nu_{\max}/\text{cm}^{-1}$  1598s  $\nu(\text{C}=\text{C} + \text{C}=\text{N})$ , 766m  $\gamma(\text{C}-\text{H})_{\text{py}}$ .  $\delta_{\text{H}}$  (300 MHz; CDCl<sub>3</sub>; Me<sub>4</sub>Si): 0.88 (12H, t, <sup>3</sup>J 6.9, CH<sub>3</sub>), 1.27 (72H, m, CH<sub>2</sub>), 1.84 (8H, qt, <sup>3</sup>J 6.7, CH<sub>2</sub>), 4.05 (8H, t, <sup>3</sup>J 6.6, OCH<sub>2</sub>), 6.43 (2H, t, <sup>4</sup>J 2.2, H<sub>p</sub>), 6.89 (2H, s, 4'-H), 7.07 (4H, d, <sup>4</sup>J 2.2, H<sub>o</sub>), 7.23 (2H, ddd, <sup>3</sup>J 7.8, 5.3, <sup>4</sup>J 1.3, 5-H), 7.58 (2H, d, <sup>3</sup>J 7.5, 3-H), 7.79 (2H, ddd, <sup>3</sup>J 7.8, 7.5, <sup>4</sup>J 1.3, 4-H), 10.38 (2H, d, <sup>3</sup>J 5.3, 6-H).  $\delta_{\text{C}}$  (75.48 MHz; CDCl<sub>3</sub>; Me<sub>4</sub>Si): 14.2 (CH<sub>3</sub>), 22.7–32.0 (CH<sub>2</sub>), 68.0 (OCH<sub>2</sub>), 99.6 (C-4'), 100.1 (C<sub>p</sub>), 103.7 (C<sub>o</sub>), 118.2 (C-3), 120.3 (C-5), 136.8 (C<sub>i</sub>), 138.6 (C-4), 149.8 (C-3'), 150.0 (C-2), 150.8 (C-6), 153.3 (C-5'), 160.3 (C<sub>m</sub>).

**Complexes [PdCl<sub>2</sub>(Hpz<sup>R(n,n)py</sup>)] (17–24).** A solution of the corresponding pyrazole [Hpz<sup>R(n,n)py</sup>] (0.26 mmol) in CH<sub>2</sub>Cl<sub>2</sub> (20 mL) was added over a solution of [PdCl<sub>2</sub>(C<sub>6</sub>H<sub>5</sub>CN)<sub>2</sub>] (0.26 mmol, 99.72 mg) in 10 mL of CH<sub>2</sub>Cl<sub>2</sub>. The reaction mixture was stirred for 24 h at reflux temperature and then filtered over celite. A pale orange solid was precipitated by the addition of acetonitrile, which was filtered off and dried *in vacuo*.

All compounds were characterised by IR, <sup>1</sup>H spectroscopies and elemental analyses (deposited as ESI†). In addition, complexes **18** and **21** were also characterised by <sup>13</sup>C-NMR as representative examples.

[PdCl<sub>2</sub>(Hpz<sup>R(6,6)py</sup>)] (**18**). Pale orange solid (57%). Found: C, 51.1; H, 5.8; N, 6.8. PdC<sub>26</sub>N<sub>3</sub>H<sub>35</sub>O<sub>2</sub>Cl<sub>2</sub>·0.2CH<sub>2</sub>Cl<sub>2</sub> requires C,

50.7; H, 5.9; N, 7.0%.  $\nu_{\max}/\text{cm}^{-1}$  3184w  $\nu(\text{N}-\text{H})$ , 1600s  $\nu(\text{C}=\text{C} + \text{C}=\text{N})$ , 770m  $\gamma(\text{C}-\text{H})_{\text{py}}$ .  $\delta_{\text{H}}$  (300 MHz; CDCl<sub>3</sub>; Me<sub>4</sub>Si): 0.92 (6H, t, <sup>3</sup>J 6.6, CH<sub>3</sub>), 1.38 (8H, m, CH<sub>2</sub>), 1.48 (4H, m, CH<sub>2</sub>), 1.84 (4H, qt, <sup>3</sup>J 6.7, CH<sub>2</sub>), 4.00 (4H, t, <sup>3</sup>J 6.3, OCH<sub>2</sub>), 5.30 (s, CH<sub>2</sub>Cl<sub>2</sub>), 6.55 (1H, t, <sup>4</sup>J 2.1, H<sub>p</sub>), 6.66 (2H, d, <sup>4</sup>J 2.1, H<sub>o</sub>), 7.04 (1H, s, 4'-H), 7.43 (1H, ddd, <sup>3</sup>J 7.7, 5.7, <sup>4</sup>J 1.2, 5-H), 7.85 (1H, d, <sup>3</sup>J 7.6, 3-H), 8.07 (1H, ddd, <sup>3</sup>J 7.7, 7.6, <sup>4</sup>J 1.4, 4-H), 9.09 (1H, d, <sup>3</sup>J 5.7, 6-H), 11.26 (1H, s, NH).  $\delta_{\text{C}}$  (75.48 MHz; CDCl<sub>3</sub>; Me<sub>4</sub>Si): 14.0 (CH<sub>3</sub>), 22.5 (CH<sub>2</sub>), 25.6 (CH<sub>2</sub>), 29.1 (CH<sub>2</sub>), 31.5 (CH<sub>2</sub>), 68.5 (OCH<sub>2</sub>), 102.0 (C-4'), 103.5 (C<sub>p</sub>), 104.3 (C<sub>o</sub>), 122.5 (C-3), 124.8 (C-5), 127.4 (C<sub>i</sub>), 140.5 (C-4), 146.0 (C-3'), 150.4 (C-6), 150.6 (C-2), 151.9 (C-5'), 161.0 (C<sub>m</sub>).

[PdCl<sub>2</sub>(Hpz<sup>R(12,12)py</sup>)] (**21**). Pale orange solid (63%). Found: C, 59.5; H, 7.7; N, 5.5. PdC<sub>38</sub>N<sub>3</sub>H<sub>59</sub>O<sub>2</sub>Cl<sub>2</sub> requires C, 59.5; H, 7.5; N, 5.6%.  $\nu_{\max}/\text{cm}^{-1}$  3187w  $\nu(\text{N}-\text{H})$ , 1598s  $\nu(\text{C}=\text{C} + \text{C}=\text{N})$ , 771m  $\gamma(\text{C}-\text{H})_{\text{py}}$ .  $\delta_{\text{H}}$  (300 MHz; CDCl<sub>3</sub>; Me<sub>4</sub>Si): 0.88 (6H, t, <sup>3</sup>J 6.6, CH<sub>3</sub>), 1.27 (32H, m, CH<sub>2</sub>), 1.46 (4H, m, CH<sub>2</sub>), 1.78 (4H, m, CH<sub>2</sub>), 3.96 (4H, t, <sup>3</sup>J 6.6, OCH<sub>2</sub>), 6.51 (1H, t, <sup>4</sup>J 2.2, H<sub>p</sub>), 6.65 (2H, d, <sup>4</sup>J 2.2, H<sub>o</sub>), 7.07 (1H, s, 4'-H), 7.41 (1H, ddd, <sup>3</sup>J 7.8, 5.5, <sup>4</sup>J 1.3, 5-H), 7.90 (1H, d, <sup>3</sup>J 7.8, 3-H), 8.08 (1H, ddd, <sup>3</sup>J 7.8, 7.7, <sup>4</sup>J 1.3, 4-H), 9.01 (1H, d, <sup>3</sup>J 5.5, 6-H), 11.32 (1H, s, NH).  $\delta_{\text{C}}$  (75.48 MHz; CDCl<sub>3</sub>; Me<sub>4</sub>Si): 14.0 (CH<sub>3</sub>), 22.6–31.8 (CH<sub>2</sub>), 68.5 (OCH<sub>2</sub>), 102.1 (C-4'), 103.6 (C<sub>p</sub>), 104.2 (C<sub>o</sub>), 122.6 (C-3), 124.9 (C-5), 127.4 (C<sub>i</sub>), 140.5 (C-4), 145.9 (C-3'), 150.3 (C-6), 150.6 (C-2), 151.9 (C-5'), 161.0 (C<sub>m</sub>).

### X-ray crystal structure determination

Data collection for all compounds was carried out at room temperature on a Bruker Smart CCD diffractometer using graphite-monochromated Mo-K $\alpha$  radiation ( $\lambda = 0.71073 \text{ \AA}$ ) operating at 50 kV and 20 mA for **1** and 50 kV and 35 mA for **12**. In both cases, data were collected over a hemisphere of the reciprocal space by combination of three exposure sets. Each exposure was of 20 s covered 0.3° in  $\omega$ . The cell parameters were determined and refined by a least-squares fit of all reflections.

The first 100 frames were recollected at the end of the data collection to monitor crystal decay, and no appreciable decay was observed. A summary of the fundamental crystal and refinement data is given in Table 5.

The structures were solved by direct methods and refined by full-matrix least-square procedures on  $F^2$ .<sup>39</sup> All non-hydrogen atoms were refined anisotropically. Despite the high quality of the crystals obtained by different crystallisation methods, the structure of **12** could not be refined further because of its poor diffraction, as indicated by the  $R_{\text{int}}$  value.

The hydrogen H1 linked to N1 for **1** was located in a Fourier synthesis and refined riding on its N-bonded atom. The remaining hydrogen atoms were included in their calculated positions and refined as riding on the respective carbon atoms. For **12** some of the C-atoms from the chains were refined using geometric restraints and variable common C–C distances.

Further crystallographic details for the structure reported in this paper may be obtained from the Cambridge Crystallo-

**Table 5** Crystal and refinement data for [Hpz<sup>R(4,4)py</sup>] **1** and [Pd(pz<sup>R(10,10)py</sup>)<sub>2</sub>] **12**

	<b>1</b>	<b>12</b>
Empirical formula	[C <sub>22</sub> H <sub>27</sub> N <sub>3</sub> O <sub>2</sub> ]	[C <sub>68</sub> H <sub>100</sub> N <sub>6</sub> O <sub>4</sub> Pd]
Formula weight	365.47	1171.94
Crystal system	Monoclinic	Triclinic
Space group	<i>P</i> 2 <sub>1</sub> / <i>n</i>	<i>P</i> 1
Space group number	11	2
<i>a</i> /Å	8.771(1)	6.785(2)
<i>b</i> /Å	21.741(2)	14.665(5)
<i>c</i> /Å	11.139(1)	18.048(5)
$\alpha$ (°)	90	67.868(6)
$\beta$ (°)	103.364(2)	83.627(7)
$\gamma$ (°)	90	82.800(7)
<i>V</i> /Å <sup>3</sup>	2066.6(3)	1646.3(9)
<i>Z</i>	4	1
<i>T</i> /K	293(2)	296(2)
<i>F</i> (000)	784	628
$\rho_c$ /g cm <sup>-3</sup>	1.175	1.182
$\mu$ /mm <sup>-1</sup>	0.076	0.331
Scan technique	$\omega$ and $\phi$	$\omega$ and $\phi$
Data collected	(-10, -25, -14) to (11, 27, 14)	(-8, -17, -21) to (7, 16, 21)
$\theta$ Range (°)	1.87 to 27.00	1.22 to 25.00
Reflections collected	18 199	11 266
Independent reflections	4507 ( <i>R</i> <sub>int</sub> = 0.0493)	5635 ( <i>R</i> <sub>int</sub> = 0.1462)
Completeness to maximum $\theta$ (%)	100	97.3
Data/restraints/parameters	4507/0/244	5635/13/346
Observed reflections [ <i>I</i> > 2 $\sigma$ ( <i>I</i> )]	1497	1597
<i>R</i> <sup>a</sup>	0.0470	0.0717
<i>R</i> <sub>w</sub> <sup>b</sup>	0.1532	0.1394

$$^a \sum[|F_o| - |F_c|] / \sum[|F_o|]. \quad ^b \{ \sum[w(F_o^2 - F_c^2)^2] / \sum[w(F_o^2)] \}^{1/2}.$$

graphic Data Centre, on quoting the depository number CCDC 977934 (**1**) and 977935 (**12**).

A preliminary study of **17** shows the square-planar environment around the metal centre of the complexes **II** (Fig. S2 in the ESI†).

## Acknowledgements

The authors are grateful to the Ministerio de Economía y Competitividad (Spain), project CTQ2011-25172.

## Notes and references

- B. Donnio, D. Guillon, R. Deschenaux and D. W. Bruce, in *Comprehensive Coordination Chemistry II*, ed. J. A. McCleverty and T. J. Meyer, Elsevier, Oxford, 2003, vol. 7, pp. 357–627.
- B. J. Coe, in *Comprehensive Coordination Chemistry II*, ed. J. A. McCleverty and T. J. Meyer, Elsevier, Oxford, 2003, vol. 9, pp. 621–687.
- G. Schweicher, G. Gbabode, F. Quist, O. Debever, N. Dumont, S. Sergeev and Y. H. Geerts, *Chem. Mater.*, 2009, **21**, 5867.
- B. Zhao, B. Liu, R. Q. Png, K. Zhang, K. A. Lim, J. Luo, J. Shao, P. K. H. Ho, C. Chi and J. Wu, *Chem. Mater.*, 2010, **22**, 435.
- T. D. Choudhury, N. V. S. Rao, R. Tenent, J. Blackburn, B. Gregg and I. I. Smalyukh, *J. Phys. Chem. B*, 2011, **115**, 609.
- R. Cristiano, D. M. P. D. Santos, G. Conte and H. Gallardo, *Liq. Cryst.*, 2006, **33**, 997.
- A. Stracke, J. H. Wendorff, D. Janietz and S. Mahlstedt, *Adv. Mater.*, 1999, **11**, 667.
- S. Sergeev, W. Pisulab and Y. H. Geerts, *Chem. Soc. Rev.*, 2007, **36**, 1902.
- A. A. Vieira, R. Cristiano, A. J. Bortoluzzi and H. Gallardo, *J. Mol. Struct.*, 2008, **875**, 364.
- P. Ovejero, E. Asensio, J. V. Heras, J. A. Campo, M. Cano, M. R. Torres, C. Núñez and C. Lodeiro, *Dalton Trans.*, 2013, **42**, 2107.
- J. A. Passo, G. D. Vilela, P. H. Schneider, O. M. S. Ritter and A. A. Merlo, *Liq. Cryst.*, 2008, **35**, 833.
- J. S. Hall, J. G. Loeb, K. H. Shimizu and G. P. A. Yap, *Angew. Chem., Int. Ed.*, 1998, **37**, 121.
- R. D. Schnebeck, E. Freisinger and B. Lippert, *Angew. Chem., Int. Ed.*, 1999, **38**, 168.
- C.-R. Wen, Y.-J. Wang, H.-C. Wang, H.-S. Sheu, G.-H. Lee and C. K. Lai, *Chem. Mater.*, 2005, **17**, 1646.
- C.-W. Chien, K.-T. Liu and C. K. Lai, *J. Mater. Chem.*, 2003, **13**, 1588.
- H.-C. Chang, K. Komasa, K. Kishida, T. Shiozaki, T. Ohmori, T. Matsumoto, A. Kobayashi, M. Kato and S. Kitagawa, *Inorg. Chem.*, 2001, **50**, 4279.
- C.-T. Liao, H.-H. Chen, H.-F. Hsu, A. Poloek, H.-H. Yeh, Y. Chi, K.-W. Wang, C.-H. Lai, G.-H. Lee, C.-W. Shih and P.-T. Chou, *Chem. Eur. J.*, 2011, **17**, 546.
- C. K. Lai, C.-H. Tsai and Y.-S. Pang, *J. Mater. Chem.*, 2008, **8**, 1355.
- K. Ohta, H. Muroki, A. Takagi, K. Hatada, H. Ema, I. Yamamoto and K. Matsuzaki, *Mol. Cryst. Liq. Cryst.*, 1986, **140**, 131.
- K. Usha, K. Vijayani and S. Chandrasekhar, *Liq. Cryst.*, 1993, **15**, 575.
- Y. Abe, H. Akao, Y. Yoshida, H. Takashima, T. Tanase, H. Mukai and K. Ohta, *Inorg. Chim. Acta*, 2006, **359**, 3147.
- M. Seredyuk, A. B. Gaspar, V. Ksenofontov, Y. Galyametdinov, M. Verdager, F. Villain and P. Gülich, *Inorg. Chem.*, 2008, **47**, 10232.
- Y. Abe, Y. Takagi, M. Nakamura, T. Takeuchi, T. Tanase, M. Yokokawa, H. Mukai, T. Megumi, A. Hachisuga and K. Ohta, *Inorg. Chim. Acta*, 2012, **392**, 254.
- W. Zhang, J.-H. Liu, J.-X. Pan, P. Li and L.-C. Sun, *Polyhedron*, 2008, **27**, 1168.
- M. C. Torralba, M. Cano, S. Gómez, J. A. Campo, J. V. Heras, J. Perles and C. Ruiz-Valero, *J. Organomet. Chem.*, 2003, **682**, 26.
- M. C. Torralba, M. Cano, J. A. Campo, J. V. Heras, E. Pinilla and M. R. Torres, *Inorg. Chem. Commun.*, 2006, **9**, 1271.

- 27 P. Ovejero, M. J. Mayoral, M. Cano and M. C. Lagunas, *J. Organomet. Chem.*, 2007, **692**, 1690.
- 28 (a) J. Barberá, A. Elduque, R. Giménez, L. A. Oro and J. L. Serrano, *Angew. Chem., Int. Ed.*, 1996, **35**, 2832; (b) J. Barberá, A. Elduque, R. Giménez, F. J. Lahoz, J. A. López, L. A. Oro and J. L. Serrano, *Inorg. Chem.*, 1998, **37**, 2960.
- 29 S. J. Kim, S. H. Kang, K.-M. Park, H. Kim, W.-C. Zin, M.-G. Choi and K. Kim, *Chem. Mater.*, 1998, **10**, 1889.
- 30 M. J. Mayoral, P. Ovejero, J. A. Campo, J. V. Heras, M. R. Torres, C. Lodeiro and M. Cano, *New J. Chem.*, 2010, **34**, 2766.
- 31 C. Cuerva, P. Ovejero, J. A. Campo and M. Cano, *New J. Chem.*, 2014, **38**, 511.
- 32 (a) M. C. Torralba, M. Cano, J. A. Campo, J. V. Heras and E. Pinilla, *Z. Kristallogr. – New Cryst. Struct.*, 2005, **220**, 617; (b) J. A. Campo, M. Cano, J. V. Heras, M. C. Lagunas, J. Perles, E. Pinilla and M. R. Torres, *Helv. Chim. Acta*, 2002, **85**, 1079.
- 33 B. P. Buffin, E. B. Fonger and A. Kundu, *Inorg. Chim. Acta*, 2003, **355**, 340.
- 34 E.-J. Sun, Z.-Y. Sun, M. Yuan, D. Wang and T.-S. Shi, *Dyes Pigm.*, 2009, **81**, 124.
- 35 H. Lee, D. Kim, H.-K. Lee, W. Qiu, N.-K. Oh, W.-C. Zin and K. Kim, *Tetrahedron Lett.*, 2004, **45**, 1019.
- 36 C. Cordovilla, S. Coco, P. Espinet and B. Donnio, *J. Am. Chem. Soc.*, 2010, **132**, 1424.
- 37 H. Gallardo, M. Ferreira, A. A. Vieira, E. Westphal, F. Molin, J. Eccher and I. H. Bechtold, *Tetrahedron*, 2011, **67**, 9491.
- 38 M. C. Torralba, M. Cano, J. A. Campo, J. V. Heras, E. Pinilla and M. R. Torres, *J. Organomet. Chem.*, 2002, **654**, 150.
- 39 G. M. Sheldrick, *SHELX97, Program for Refinement of Crystal Structure*, University of Göttingen, Göttingen, 1997.